Octupolar versus Néel Order in Cubic $5d^2$ Double Perovskites

D. D. Maharaj,[1,*] G. Sala,[1,2] M. B. Stone,[2] E. Kermarrec,[1,3] C. Ritter,[4] F. Fauth,[5] C. A. Marjerrison,[6] J. E. Greedan,[6,7] A. Paramekanti,[8] and B. D. Gaulin[1,6,9]

[1]*Department of Physics and Astronomy, McMaster University, Hamilton, Ontario L8S 4M1, Canada*
[2]*Neutron Scattering Division, Oak Ridge National Laboratory, Oak Ridge, Tennessee 37831, USA*
[3]*Université Paris-Saclay, CNRS, Laboratoire de Physique des Solides, 91405 Orsay, France*
[4]*Institut Laue-Langevin, Boîte Postale 156, 38042 Grenoble Cédex, France*
[5]*CELLS-ALBA Synchrotron, Carrer de la Llum 2-26, 08290 Cerdanyola del Vallès, Barcelona, Spain*
[6]*Brockhouse Institute for Materials Research, McMaster University, Hamilton, Ontario L8S 4M1, Canada*
[7]*Department of Chemistry and Chemical Biology, McMaster University, Ontario L8S 4M1, Canada*
[8]*Department of Physics, University of Toronto, 60 St. George Street, Toronto, Ontario M5S 1A7, Canada*
[9]*Canadian Institute for Advanced Research, 661 University Avenue, Toronto, Ontario M5G 1M1, Canada*

(Received 6 September 2019; accepted 30 January 2020; published 27 February 2020)

We report time-of-flight neutron spectroscopy and neutron and x-ray diffraction studies of the $5d^2$ double perovskite magnets, Ba_2MOsO_6 ($M = Zn, Mg, Ca$). These materials host antiferromagnetically coupled $5d^2$ Os^{6+} ions decorating a face-centered cubic (fcc) lattice and are found to remain cubic down to the lowest temperatures. They all exhibit thermodynamic anomalies consistent with a single phase transition at a temperature T^*, and a gapped magnetic excitation spectrum with spectral weight concentrated at wave vectors typical of type-I antiferromagnetic orders. However, while muon spin resonance experiments show clear evidence for time-reversal symmetry breaking below T^*, we observe no corresponding magnetic Bragg scattering signal. These results are shown to be consistent with ferro-octupolar symmetry breaking below T^*, and are discussed in the context of other $5d$ double perovskite magnets and theories of exotic orders driven by multipolar interactions.

DOI: 10.1103/PhysRevLett.124.087206

Introduction.—Ordered double perovskite magnets, with the chemical formula $A_2BB'O_6$, provide a fascinating avenue to study the interplay of geometric frustration with strong spin-orbit coupling [1]. Here, B and B' sublattices individually form a fcc lattice of edge-sharing tetrahedra, an archetype for geometric frustration in three dimensions. Furthermore, the flexibility of the double perovskite lattice to host heavy ions at the B' site allows the study of spin-orbit driven physics, as the strength of spin-orbit coupling scales $\sim Z^2$, where Z is the atomic number of the magnetic ion [2]. This interplay of spin-orbit coupling and frustration in double perovskites is predicted to yield exotic ground states [3–6].

The single-particle t_{2g} levels in an octahedral crystal field are split by strong spin-orbit coupling, resulting in a quartet $j = 3/2$ ground state and a doublet $j = 1/2$ excited state. Famously, for a d^5 electronic configuration, as occurs for Ir^{4+} or Ru^{3+}, this results in a single $j = 1/2$ hole, leading to extreme quantum magnetism, and Kitaev exchange interactions in appropriate geometries [7–13]. On the other hand, ions with d^1 and d^2 configurations are, respectively, expected to form $j = 3/2$ or total $J = 2$ moments [3,4,6]. Theoretical studies incorporating intersite orbital repulsion between such ions argue for wide regimes of quadrupolar order on the fcc lattice [3,4,6] which may coexist with dipolar antiferromagnetic or valence bond orders [14]. Recent experiments on $5d^1$ oxides, Ba_2NaOsO_6 with Os^{7+} [15,16] and Ba_2MgReO_6 with Re^{6+} [17], have found evidence for two transitions associated with these distinct broken symmetries: quadrupolar ordering at T_Q and onset of coexisting dipolar antiferromagnetic order below a lower transition temperature T_N.

In this Letter, we explore the case of d^2 ions on the B' site, with effective $J = 2$ moments. We report new magnetic neutron powder diffraction, inelastic neutron scattering, and high angular resolution synchrotron x-ray diffraction results on three cubic double perovskites: Ba_2MOsO_6, with $M = Zn$, Mg, Ca (respectively referred to henceforth as BZO, BMO, and BCO). In contrast to d^1 double perovskites, these materials display clear thermodynamic signatures of a *single* phase transition [18–20] at $T^* \sim 30$–50 K, which is associated with time-reversal symmetry breaking based on oscillations observed in zero field muon spin relaxation (μSR) [20]. Our inelastic neutron scattering results show strong, gapped, magnetic spectral weight at wave vectors typical of type-I antiferromagnetic order, but we detect no clear signature of an ordered antiferromagnetic moment in the diffraction data, leading us to place an upper limit between 0.13 and $0.06\mu_B$ per B' site. Furthermore, our neutron powder diffraction

and x-ray diffraction results show no deviation from cubic symmetry, thus ruling out quadrupolar order. We propose that these striking and unexpected results may be understood via the emergence of time-reversal symmetry breaking ferro-octupolar order below T^*.

Multipolar orders have been extensively studied in heavy fermion f-electron compounds [21]. Examples include NpO_2 [22–25], where experiments suggest a primary rank-5 magnetic multipolar order driving secondary quadrupolar order, the "hidden order" state of URu_2Si_2 [26–28], and recent discoveries of quadrupolar and octupolar orders in PrX_2Al_{20} ($X = \mathrm{Ti}, \mathrm{V}$) [29–31]. In stark contrast, multipolar orders in d-electron systems are less explored [15–17,32–34]; our work appears to be the first reported candidate for d-orbital octupolar order.

BZO, BMO, and BCO have been previously studied in powder form. In all three materials, neutron powder diffraction and x-ray diffraction confirm that they remain in the cubic $Fm\bar{3}m$ space group down to the lowest temperature. They all display Curie-Weiss-like magnetic susceptibilities (χ) at high temperatures, with large antiferromagnetic Curie-Weiss constants ($\Theta_{\mathrm{CW}} \sim 130\,\mathrm{K}$), and anomalies at T^* in the form of a splitting between field-cooled and zero-field-cooled results. They all exhibit peaks in their heat capacity, or in the related measure $d(\chi T)/dT$, at $T^* \sim 50$ K (BMO, BCO) or $T^* \sim 30$ K (BZO), indicating a phase transition [18,20]. These findings are summarized in Table I.

The entropy released up to $\sim 2T^*$ in all three materials appears to be $\sim R\ln(2)$ per mole, as explicitly shown for BZO and BMO in the Supplemental Material [35,36]. This is much smaller than the $R\ln(5)$ expected for an effective $J = 2$ moment [18–20], and it points to part of the entropy being quenched at $T \gg T^*$ (i.e., above ~200 K). This is in contrast to the $\sim R\ln(5)$ entropy released up to $\sim 2T_N$ for the tetragonal counterpart Sr_2MgOsO_6, which has a high Néel ordering temperature $T_N \sim 100$ K [37].

These three cubic samples have also been previously studied using μSR techniques [18,20], and it is primarily on the basis of these zero longitudinal field μSR oscillations for $T < T^*$, indicative of a time-reversal broken state, that the transition at T^* was associated with antiferromagnetic order. However, no magnetic neutron diffraction peaks could be identified in this earlier study at low temperatures, with a sensitivity to ordered moment of $\sim 0.7\ \mu_B$. In the present work, we *significantly* improve on this bound, still finding no evidence of magnetic Bragg peaks.

TABLE I. Summary of experimental results for the three cubic double perovskites studied. T^* denotes the peak in the heat capacity indicating a thermodynamic phase transition [18,20]. θ_{CW} is the Curie-Weiss temperature extracted from high temperature susceptibility data [18,20]. μ_{ord} is the upper limit on the ordered dipolar moment associated with type-I antiferromagnetic order, as determined from neutron diffraction in this work.

System	T^*	θ_{CW}	a (Å)	Reference	μ_{ord}
Ba_2CaOsO_6	49	−156.2(3)	8.3456	[18]	$<0.13\ \mu_B$
Ba_2MgOsO_6	51	−120(1)	8.0586	[20]	$<0.11\ \mu_B$
Ba_2ZnOsO_6	30	−149.0(4)	8.0786	[20]	$<0.06\ \mu_B$

The corresponding $5d^3$ osmium-based double perovskites, both cubic Ba_2YOsO_6 and monoclinic Sr_2ScOsO_6 and La_2LiOsO_6, show clear Néel transitions to antiferromagnetic ordered states, with large ordered moments $\sim 1.7\mu_B$ [19,38–41]. These observed ordered moments are reduced from the $3\mu_B$ value expected for an orbitally quenched moment, pointing to strong spin-orbit coupling effects, or covalency, or both. Nonetheless, magnetic Bragg scattering at the (100) and (110) positions is easily observed, along with strong, gapped inelastic magnetic scattering centered at these two ordering wave vectors. Previously studied $5d^2$ double perovskites such as monoclinic Sr_2MgOsO_6 and cubic Ba_2LuReO_6 (with Re^{5+}) also show transitions to type-I antiferromagnetic order, as seen via neutron diffraction, albeit with much smaller ordered moments, 0.6(2) and 0.34(4) μ_B, respectively [37,42].

Below we present our experimental findings on powder samples of the cubic systems, BZO, BMO, and BCO. Details of experimental methods and analysis are in the Supplemental Material [35], which includes Refs. [43–47]. Our new neutron powder diffraction measurements on D20 [48,49] at the Institut Laue Langevin (ILL) have ~10–20 times more sensitivity to magnetic Bragg scattering as compared with previous neutron powder diffraction measurements taken at the C2 instrument of the Chalk River Laboratories. No magnetic Bragg scattering is observed at 10 K, factors of 3–5 below T^* for any of these materials. We do, however, observe gapped, inelastic magnetic spectral weight centered on wave vectors characteristic of type-I antiferromagnetic order. We thus conclude that the dominant broken symmetry below T^* in these three cubic double perovskite d^2 magnets must involve multipolar ordering.

Results.—Time-of-flight inelastic neutron scattering measurements from SEQUOIA [50] are shown in Fig. 1. Figures 1(a)–1(c) show the inelastic neutron scattering spectra well below (top panel) and above (bottom panel) T^* for BZO, BMO, and BCO, respectively. Figures 1(d)–1(f) show cuts through this data as a function of energy, integrating all $|Q| < 1.15$ Å^{-1}, and as a function of temperature, again for BZO, BMO, and BCO respectively.

The datasets for all three samples in Fig. 1 are similar, with gapped magnetic spectral weight at low $|Q|$'s, typical of the 100 (0.78 Å^{-1}) and 110 (1.1 Å^{-1}) Bragg positions. The full bandwidth of the magnetic excitation spectrum appears to be ~6 meV. From Figs. 1(b), 1(c), 1(e), and 1(f), this magnetic spectral weight overlaps in energy with strong phonon scattering near ~18 and 14 meV for BMO and BCO, respectively. Even though our low $|Q|$ integration favors magnetic scattering at the expense of

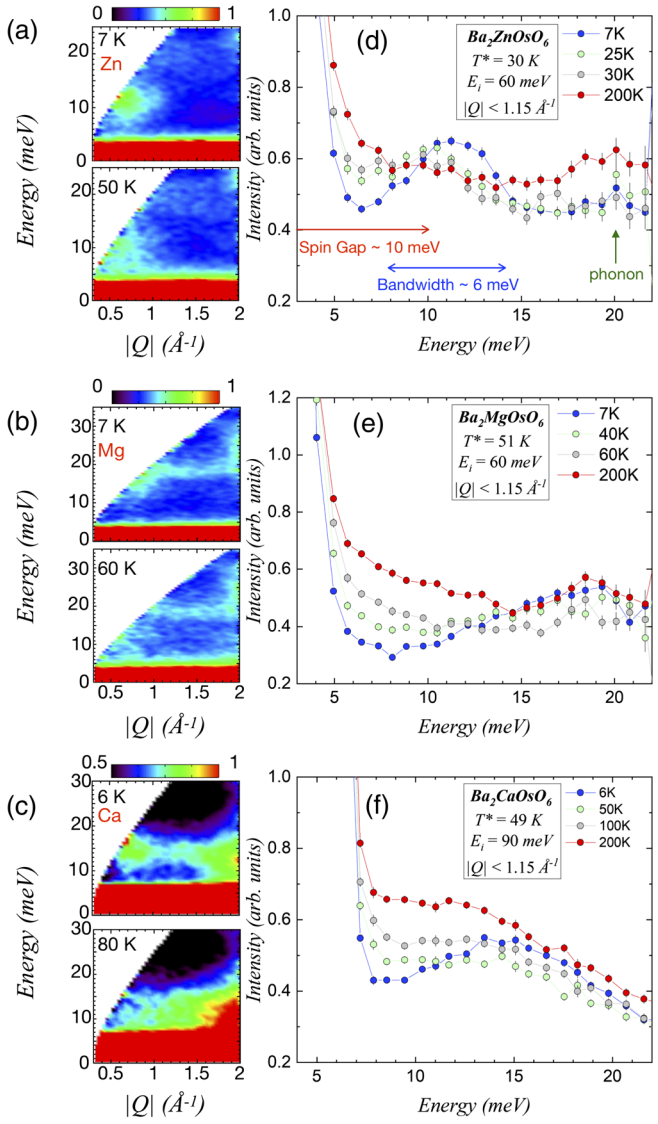

FIG. 1. (a)–(c) Neutron scattering intensity contour plots for BZO, BMO, and BCO shown as a function of energy transfer E and momentum transfer $|Q|$ at base temperature (top) and at $T > T^*$ (bottom), respectively. Below T^*, clear gapped magnetic inelastic spectral weight develops around (100) and (110) wave vectors (~0.78 $Å^{-1}$) and 110 (1.1 $Å^{-1}$) in each case. (d),(e) Low $|Q|$ integrated cuts of the neutron scattering intensity as a function of energy transfer E as a function of temperature for BZO, BMO, and BCO, respectively. A gap in the magnetic excitation spectrum is clearly revealed for each compound for $T < T^*$.

scattering from phonons, whose intensity tends to go like $|Q|^2$, we still pick up a sizable contribution from this high phonon density of states (DOS), especially at high temperatures where the thermal population of the phonons is large. The observed redshift in the peak of the phonon DOS from ~17 meV in BMO to ~14 meV for BCO is expected since Ca^{2+} is isoelectronic to Mg^{2+} but heavier. While the Zn^{2+} in BZO is heavier still than Ca^{2+}, it is not isoelectronic, instead possessing a filled $3d$ shell. This might lead to its higher energy phonon.

As the high phonon DOS is well separated from the magnetic spectral weight in BZO, shown in Figs. 1(a) and 1(d), this is where the nature of the gapped magnetic scattering is most easily appreciated. The energy cuts in Fig. 1(d) clearly show a well developed gap of ~10 meV and a bandwidth of ~6 meV. This structure collapses by 25 K, where $T^* = 30$ K for BZO, at which point the gap has largely filled in and only a vestige of an overdamped spin excitation at ~10 meV remains. This is very similar to what occurs in the d^3 double perovskites on the approach to their T_N's, *except* that there is no obvious temperature dependent Bragg scattering at the 100 or 110 positions, as would be expected for type-I antiferromagnetic order.

The absence of evidence for magnetic Bragg scattering is seen in Fig. 2. Figure 2(a) shows neutron diffraction data taken at $T = 10$ K, well below $T^* = 30$ K in BZO, using the D20 diffractometer at the ILL [48]. These data and the corresponding neutron powder diffraction data on BMO and BCO refine in the cubic $Fm\bar{3}m$ space group at all temperatures measured. Figures 2(b)–2(d) then show a subtraction of high temperature (50 K for BZO, 70 K for BMO and BCO) datasets from low temperature data sets for each of BZO, BCO, and BMO, respectively. A calculated neutron diffraction profile appropriate for a type-I antiferromagnetic structure below T^* is shown as the red line in Figs. 2(b)–2(d), where the assumed ordered moment in the calculation is $0.06\mu_B$ for BZO [Fig. 2(b)], $0.11\mu_B$ for BMO [Fig. 2(c)], and $0.13\mu_B$ for BCO [Fig. 2(d)]. Taking the case where the evidence *against* long-range magnetic order below T^* is most stringent, BZO, we can eliminate conventional type-I antiferromagnetic order of magnetic dipoles with an ordered moment greater than $\sim 0.06\mu_B$. This upper limit for magnetic dipole order is a factor of ~12 more stringent than previous limits on magnetic Bragg scattering for this family of cubic double perovskite materials. This upper bound for $\mu_{\rm ord}$ in BCO is ~35% lower than the value, $0.2\mu_B$, previously extracted from a comparison of the μSR internal fields of BCO and Ba_2YRuO_6 [18,51].

Competing multipolar orders.—Our study shows that all or most of the static $5d^2$ moment of Os^{6+} in BZO, BMO, and BCO is not visible to neutron diffraction below T^*. Nonetheless, strong inelastic magnetic scattering is easily observed at all temperatures, and it is most clearly gapped at $T \ll T^*$. One scenario to explain these results is that the ground state has dominant quadrupolar ordering, accompanied by weak dipolar ordering [3,4,6]. A quadrupolar ordering transition at $T \gg T^*$ can partially quench the $R\ln(5)$ entropy, with the residual $\sim R\ln(2)$ entropy being quenched by antiferromagnetic dipolar ordering at T^* which breaks time-reversal symmetry. The quadrupolar order can also pin the direction of the ordered dipole moment, explaining the spin gap, and if the ordered dipole moment is weak, it may escape detection in a neutron powder diffraction experiment. However, the orbital

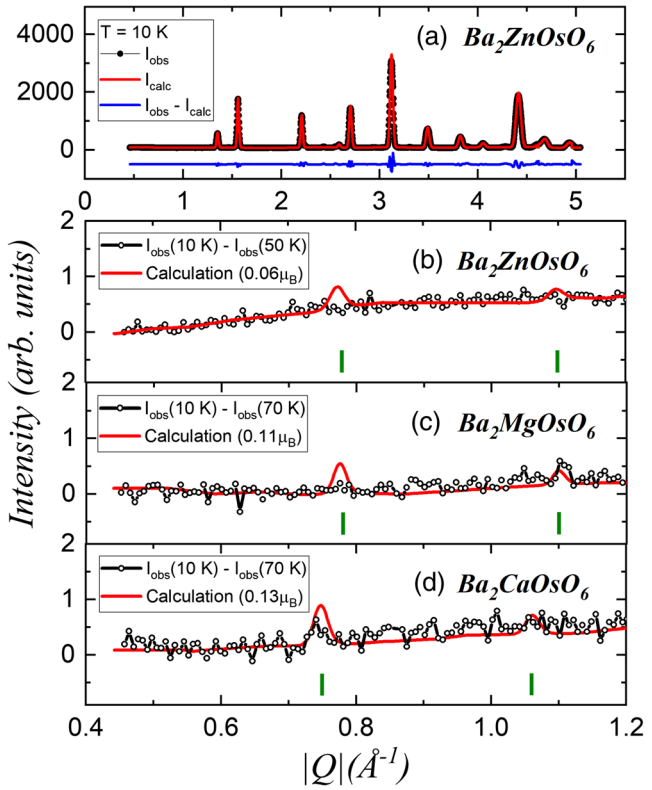

FIG. 2. (a) Neutron powder diffraction measurements on BZO for $T = 10$ K with the experimental dataset in black and the fit to the refined $Fm\bar{3}m$ structure in red. (b) Subtraction of the 50 K dataset from the 10 K dataset. The red line shows the calculated magnetic diffraction pattern for BZO with an Os^{6+} ordered moment of 0.06 μ_B, which we establish as the upper limit for an ordered dipole moment in BZO. Green fiducial lines indicate the locations of the magnetic peaks expected for type-I antiferromagnetic order. Panels (c) and (d) show the same comparison for BMO and BCO. These establish upper limits on an ordered Os^{6+} dipole moment of 0.11 and 0.13 μ_B, respectively.

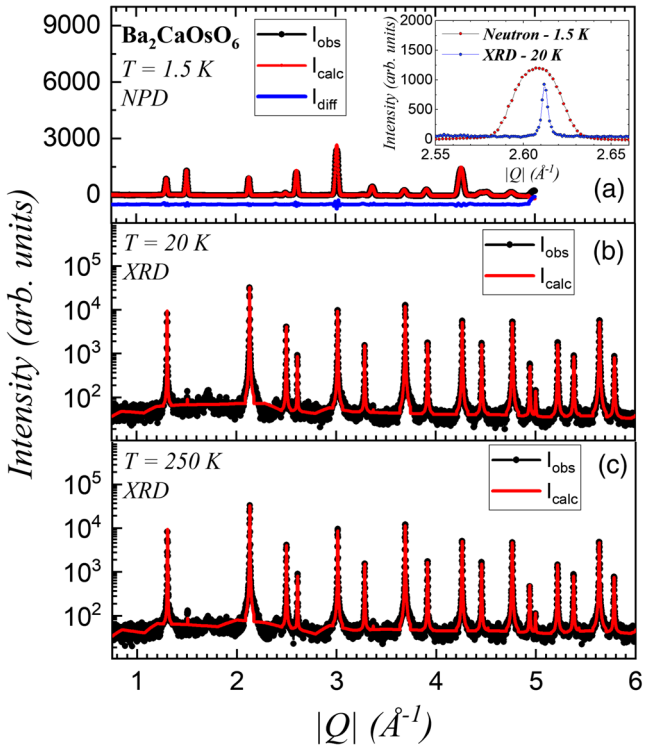

FIG. 3. (a) The neutron powder diffraction profile for BCO is shown at $T = 1.5$ K in the main panel, while the inset shows a comparison of neutron powder diffraction versus synchrotron x-ray diffraction data taken on BCO at 20 K. Panels (b) and (c) show synchrotron x-ray diffraction data on BCO at T = 20 K (b) and T = 250 K (c), along with corresponding cubic structural refinements, in red.

selection accompanying such a quadrupolar order would lower the crystal symmetry, at odds with our high resolution neutron powder diffraction data shown for BCO in Fig. 2(a). We have carried out even higher resolution x-ray diffraction measurements on BCO, the family member which best exhibits undamped zero field μSR oscillations. These measurements were conducted at the high angular resolution diffraction instrument $BL04 - MSPD$, beam line 8 of the ALBA Synchrotron Light facility (Barcelona, Spain) [52]. The sensitivity of these measurements to possible weak splittings of the cubic Bragg peaks is ~10 times greater than the neutron powder diffraction measurements; see Fig. 3(a) inset. These x-ray diffraction results, in Figs. 3(b)–3(d), show no splitting or broadening of the cubic Bragg peaks, yielding an upper limit on local distortions $< 0.1\%$ (see Supplemental Material [35]). This confirms that BCO remains cubic even for $T \ll T^*$, ruling out quadrupolar ordering. We contrast this with the $5d^1$ osmate Ba_2NaOsO_6 which exhibits measurable ~0.5%–0.7% local distortions associated with quadrupolar ordering [53].

Here, we propose a distinct scenario, an octupolar ordered ground state, that provides the most promising vehicle to explain all the salient observations. For an effective $J = 2$ moment, a residual octahedral crystal field Hamiltonian is $H_{\mathrm{CEF}'} = -V_{\mathrm{eff}}(\mathcal{O}_{40} + 5\mathcal{O}_{44})$, where the Steven's operators (dropping constant terms) are

$$\mathcal{O}_{40} = 35J_z^4 - [30J(J+1) - 25]J_z^2, \tag{1}$$

$$\mathcal{O}_{44} = \frac{1}{2}(J_+^4 + J_-^4). \tag{2}$$

$V_{\mathrm{eff}} > 0$ results in a non-Kramers ground state doublet and an excited triplet with a gap $\Delta = 120V_{\mathrm{eff}}$, as shown in Fig. 4 (details in Supplemental Material [35]). This naturally accounts for partial entropy quenching for $T \lesssim \Delta$, without a phase transition, with the residual $R\ln(2)$ entropy being quenched by ordering within the doublet sector at T^*. In the $|J_z = m\rangle$ basis, the ground state wave functions are $|\psi_{g,\uparrow}\rangle = |0\rangle$ and $|\psi_{g,\downarrow}\rangle = (1/\sqrt{2})(|2\rangle + |-2\rangle)$, with excited triplet

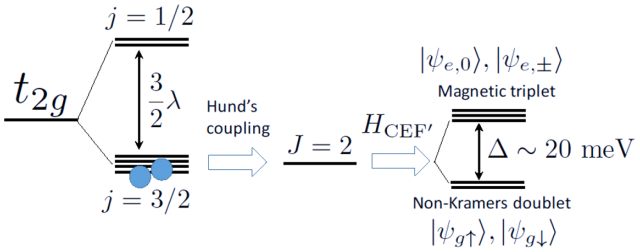

FIG. 4. Schematic level diagram showing single-particle t_{2g} orbitals split by spin-orbit coupling (λ) and interactions (Hund's coupling) leading to a $J = 2$ ground state. Residual crystal field $H_{\mathrm{CEF}'}$ splits this $J = 2$ manifold into a non-Kramers doublet ground state and an excited magnetic triplet (see text for details).

wave functions $|\psi_{e,\pm}\rangle = |\pm 1\rangle$ and $|\psi_{e,0}\rangle = (1/\sqrt{2})(|2\rangle - |-2\rangle)$. The ground state manifold has vanishing matrix elements for the dipole operators $\vec{J}$, precluding dipolar order. However, $\vec{J}$ can induce transitions into the excited triplet, accounting for the spin gap in inelastic neutron scattering. Defining pseudospin-1/2 operators $\vec{\tau}$ within the ground doublet, the quadrupolar operators are $(J_x^2 - J_y^2) \equiv 2\sqrt{3}\tau_x$, $(3J_z^2 - J^2) \equiv -6\tau_z$, while the octupolar operator $\overline{J_x J_y J_z} \equiv -\sqrt{3}\tau_y$ (overline denoting symmetrization). Octupolar order, with $\langle\tau_y\rangle \neq 0$, leads to broken time-reversal symmetry below T^* while preserving cubic symmetry. A mean field calculation with $\langle\tau_y\rangle \neq 0$ qualitatively captures the observed entropy and magnetic susceptibility (see Supplemental Material [35]). Further implications of this proposal are studied in Ref. [54].

To conclude, the low temperature phases of the cubic $5d^2$ double perovskites BZO, BMO, and BCO are best described as arising from octupolar order within a non-Kramers ground state doublet. This exotic ground state appears to require the perfect fcc structure as noncubic d^2 double perovskites, such as Sr_2MgOsO_6 [37], display conventional antiferromagnetic ground states. In noncubic systems like Sr_2MgOsO_6, the non-Kramers degeneracy is broken and antiferromagnetic exchange is stronger. Further structural studies, using dilatometry and total x-ray scattering on single crystals, and probes such as magnetostriction or Raman scattering [55], may provide smoking gun signatures of octupolar order in these $5d^2$ materials.

This work was supported by the Natural Sciences and Engineering Research Council of Canada. It was also supported in part by the National Science Foundation under Grant No. PHYS-1066293 and the hospitality of the Aspen Center for Physics. We also acknowledge the hospitality of the Telluride Science Research Center. We gratefully acknowledge useful conversations with G. M. Luke and G. Chen. We are very grateful for the instrument and sample environment support provided during our inelastic neutron scattering measurements at SEQUOIA. The experiments which were performed at the Spallation Neutron Source at Oak Ridge National Laboratory were sponsored by the U.S. Department of Energy, Office of the Basic Energy Sciences, Scientific User Facilities Division. The authors would also like to acknowledge ILL for beam time allocation experiment code 5-31-2577. We acknowledge the BL04-MSPD staff of ALBA for the x-ray synchrotron powder diffraction data collection.

*maharadd@mcmaster.ca

[1] W. Witczak-Krempa, G. Chen, Y. B. Kim, and L. Balents, Annu. Rev. Condens. Matter Phys. **5**, 57 (2014).
[2] K. V. Shanavas, Z. S. Popović, and S. Satpathy, Phys. Rev. B **90**, 165108 (2014).
[3] G. Chen, R. Pereira, and L. Balents, Phys. Rev. B **82**, 174440 (2010).
[4] G. Chen and L. Balents, Phys. Rev. B **84**, 094420 (2011).
[5] C. Svoboda, M. Randeria, and N. Trivedi, Phys. Rev. B **95**, 014409 (2017).
[6] C. Svoboda, M. Randeria, and N. Trivedi, arXiv:1702.03199.
[7] J. Chaloupka, G. Jackeli, and G. Khaliullin, Phys. Rev. Lett. **105**, 027204 (2010).
[8] Y. Singh, S. Manni, J. Reuther, T. Berlijn, R. Thomale, W. Ku, S. Trebst, and P. Gegenwart, Phys. Rev. Lett. **108**, 127203 (2012).
[9] K. W. Plumb, J. P. Clancy, L. J. Sandilands, V. V. Shankar, Y. F. Hu, K. S. Burch, H.-Y. Kee, and Y.-J. Kim, Phys. Rev. B **90**, 041112(R) (2014).
[10] S. Hwan Chun, J.-W. Kim, J. Kim, H. Zheng, C. C. Stoumpos, C. D. Malliakas, J. F. Mitchell, K. Mehlawat, Y. Singh, Y. Choi, T. Gog, A. Al-Zein, M. M. Sala, M. Krisch, J. Chaloupka, G. Jackeli, G. Khaliullin, and B. J. Kim, Nat. Phys. **11**, 462 (2015).
[11] A. Banerjee, C. A. Bridges, J. Q. Yan, A. A. Aczel, L. Li, M. B. Stone, G. E. Granroth, M. D. Lumsden, Y. Yiu, J. Knolle, S. Bhattacharjee, D. L. Kovrizhin, R. Moessner, D. A. Tennant, D. G. Mandrus, and S. E. Nagler, Nat. Mater. **15**, 733 (2016).
[12] S. M. Winter, A. A. Tsirlin, M. Daghofer, J. van den Brink, Y. Singh, P. Gegenwart, and R. Valentí, J. Phys. Condens. Matter **29**, 493002 (2017).
[13] Y. Kasahara, T. Ohnishi, Y. Mizukami, O. Tanaka, S. Ma, K. Sugii, N. Kurita, H. Tanaka, J. Nasu, Y. Motome, T. Shibauchi, and Y. Matsuda, Nature (London) **559**, 227 (2018).
[14] J. Romhányi, L. Balents, and G. Jackeli, Phys. Rev. Lett. **118**, 217202 (2017).
[15] L. Lu, M. Song, W. Liu, A. P. Reyes, P. Kuhns, H. O. Lee, I. R. Fisher, and V. F. Mitrović, Nat. Commun. **8**, 14407 (2017).
[16] W. Liu, R. Cong, E. Garcia, A. Reyes, H. Lee, I. Fisher, and V. Mitrovi, Physica (Amsterdam) **536B**, 863 (2018).
[17] D. Hirai and Z. Hiroi, J. Phys. Soc. Jpn. **88**, 064712 (2019).
[18] C. M. Thompson, J. P. Carlo, R. Flacau, T. Aharen, I. A. Leahy, J. R. Pollichemi, T. J. S. Munsie, T. Medina, G. M. Luke, J. Munevar, S. Cheung, T. Goko, Y. J. Uemura, and J. E. Greedan, J. Phys. Condens. Matter **26**, 306003 (2014).

[19] E. Kermarrec, C. A. Marjerrison, C. M. Thompson, D. D. Maharaj, K. Levin, S. Kroeker, G. E. Granroth, R. Flacau, Z. Yamani, J. E. Greedan, and B. D. Gaulin, Phys. Rev. B **91**, 075133 (2015).

[20] C. A. Marjerrison, C. M. Thompson, A. Z. Sharma, A. M. Hallas, M. N. Wilson, T. J. S. Munsie, R. Flacau, C. R. Wiebe, B. D. Gaulin, G. M. Luke, and J. E. Greedan, Phys. Rev. B **94**, 134429 (2016).

[21] P. Santini, S. Carretta, G. Amoretti, R. Caciuffo, N. Magnani, and G. H. Lander, Rev. Mod. Phys. **81**, 807 (2009).

[22] P. Santini and G. Amoretti, Phys. Rev. Lett. **85**, 2188 (2000).

[23] J. A. Paixão, C. Detlefs, M. J. Longfield, R. Caciuffo, P. Santini, N. Bernhoeft, J. Rebizant, and G. H. Lander, Phys. Rev. Lett. **89**, 187202 (2002).

[24] A. Kiss and P. Fazekas, Phys. Rev. B **68**, 174425 (2003).

[25] Y. Tokunaga, D. Aoki, Y. Homma, S. Kambe, H. Sakai, S. Ikeda, T. Fujimoto, R. E. Walstedt, H. Yasuoka, E. Yamamoto, A. Nakamura, and Y. Shiokawa, Phys. Rev. Lett. **97**, 257601 (2006).

[26] K. Haule and G. Kotliar, Nat. Phys. **5**, 796 (2009).

[27] H.-H. Kung, R. E. Baumbach, E. D. Bauer, V. K. Thorsmølle, W.-L. Zhang, K. Haule, J. A. Mydosh, and G. Blumberg, Science **347**, 1339 (2015).

[28] H.-H. Kung, S. Ran, N. Kanchanavatee, V. Krapivin, A. Lee, J. A. Mydosh, K. Haule, M. B. Maple, and G. Blumberg, Phys. Rev. Lett. **117**, 227601 (2016).

[29] A. Sakai and S. Nakatsuji, J. Phys. Soc. Jpn. **80**, 063701 (2011).

[30] T. J. Sato, S. Ibuka, Y. Nambu, T. Yamazaki, T. Hong, A. Sakai, and S. Nakatsuji, Phys. Rev. B **86**, 184419 (2012).

[31] M. Tsujimoto, Y. Matsumoto, T. Tomita, A. Sakai, and S. Nakatsuji, Phys. Rev. Lett. **113**, 267001 (2014).

[32] L. Fu, Phys. Rev. Lett. **115**, 026401 (2015).

[33] J. W. Harter, Z. Y. Zhao, J.-Q. Yan, D. G. Mandrus, and D. Hsieh, Science **356**, 295 (2017).

[34] S. Hayami, H. Kusunose, and Y. Motome, Phys. Rev. B **97**, 024414 (2018).

[35] See Supplemental Material at http://link.aps.org/supplemental/10.1103/PhysRevLett.124.087206 for experiment details (Part I), time-of-flight inelastic neutron scattering (Part I A), high intensity neutron powder diffraction (Part I B), high angular resolution x-ray diffraction (Part I C), theory (Part II), and the single-site model, multipole moments (Part II A).

[36] K. Yamamura, M. Wakeshima, and Y. Hinatsu, J. Solid State Chem. **179**, 605 (2006).

[37] R. Morrow, A. E. Taylor, D. J. Singh, J. Xiong, S. Rodan, A. U. B. Wolter, S. Wurmehl, B. Büchner, M. B. Stone, A. I. Kolesnikov, A. A. Aczel, A. D. Christianson, and P. M. Woodward, Sci. Rep. **6**, 32462 (2016).

[38] D. D. Maharaj, G. Sala, C. A. Marjerrison, M. B. Stone, J. E. Greedan, and B. D. Gaulin, Phys. Rev. B **98**, 104434 (2018).

[39] A. E. Taylor, R. Morrow, D. J. Singh, S. Calder, M. D. Lumsden, P. M. Woodward, and A. D. Christianson, Phys. Rev. B **91**, 100406(R) (2015).

[40] C. M. Thompson, C. A. Marjerrison, A. Z. Sharma, C. R. Wiebe, D. D. Maharaj, G. Sala, R. Flacau, A. M. Hallas, Y. Cai, B. D. Gaulin, G. M. Luke, and J. E. Greedan, Phys. Rev. B **93**, 014431 (2016).

[41] A. A. Aczel, D. E. Bugaris, L. Li, J.-Q. Yan, C. de la Cruz, H. C. zur Loye, and S. E. Nagler, Phys. Rev. B **87**, 014435 (2013).

[42] J. Xiong, J. Yan, A. A. Aczel, and P. M. Woodward, J. Solid State Chem. **258**, 762 (2018).

[43] R. T. Azuah, L. R. Kneller, Y. Qiu, P. L. W. Tregenna-Piggott, C. M. Brown, J. R. D. Copley, and R. M. Dimeo, J. Res. Natl. Inst. Stand. Technol. **114**, 341 (2009).

[44] O. Arnold *et al.*, Nucl. Instrum. Methods Phys. Res., Sect. A **764**, 156 (2014).

[45] J. Rodriguez-Carvajal, Physica (Amsterdam) **192B**, 55 (1993).

[46] K. Kobayashi, T. Nagao, and M. Ito, Acta Crystallogr. Sect. A **67**, 473 (2011).

[47] P. J. van der Linden, M. Moretti Sala, C. Henriquet, M. Rossi, F. Ohgushi, K. Fauth, L. Simonelli, C. Marini, E. Fraga, C. Murray, J. Potter, and M. Krisch, Rev. Sci. Instrum. **87**, 115103 (2016).

[48] T. C. Hansen, P. F. Henry, H. E. Fischer, J. Torregrossa, and P. Convert, Meas. Sci. Technol. **19**, 034001 (2008).

[49] E. Kermarrec, B. D. Gaulin, M. Dalini, and R. Clemens, *Magnetic Ordering and Ground State Selection in the Frustrated 5d2 and 5d1 FCC Double Perovskites A2BB'O6 with Neutron Diffraction* (Institut Laue-Langevin, 2018), https://doi.ill.fr/10.5291/ILL-DATA.5-31-2577.

[50] G. E. Granroth, A. I. Kolesnikov, T. E. Sherline, J. P. Clancy, K. A. Ross, J. P. C. Ruff, B. D. Gaulin, and S. E. Nagler, J. Phys. Conf. Ser. **251**, 012058 (2010).

[51] J. P. Carlo, J. P. Clancy, K. Fritsch, C. A. Marjerrison, G. E. Granroth, J. E. Greedan, H. A. Dabkowska, and B. D. Gaulin, Phys. Rev. B **88**, 024418 (2013).

[52] F. Fauth, I. Peral, C. Popescu, and M. Knapp, Powder Diffr. **28**, S360 (2013).

[53] W. Liu, R. Cong, A. P. Reyes, I. R. Fisher, and V. F. Mitrović, Phys. Rev. B **97**, 224103 (2018).

[54] A. Paramekanti, D. D. Maharaj, and B. D. Gaulin, companion paper, Phys. Rev. B **101**, 054439 (2020).

[55] A. S. Patri, A. Sakai, S. Lee, A. Paramekanti, S. Nakatsuji, and Y. B. Kim, Nat. Commun. **10**, 4092 (2019).